Targeted synthesis of trimeric organic-bromoplumbate hybrids that display intrinsic, highly Stokes-shifted, broadband emission

Benny Febriansyah,[a,b,c] Chong Shern Daniel Neo,[a] David Giovanni,[d] Shivani Srivastava,[e] Yulia Lekina,[d] Teck Ming Koh,[b] Yongxin Li,[a] Ze Xiang Shen,[d] Mark Asta,[e] Tze Chien Sum,[d] Nripan Mathews[b,f*] and Jason England.[a*]

[a]Division of Chemistry and Biological Chemistry, School of Physical and Mathematical Sciences, Nanyang Technological University, 21 Nanyang Link, Singapore 637371.

[b]Energy Research Institute at Nanyang Technological University (ERI@N), Research Techno Plaza, X-Frontier Block Level 5, 50 Nanyang Drive, Singapore 637553.

[c]Interdisciplinary Graduate School (IGS), Nanyang Technological University, 50 Nanyang Avenue, Singapore 639798.

[d]Division of Physics and Applied Physics, School of Physical and Mathematical Sciences, Nanyang Technological University, 21 Nanyang Link, Singapore 63737.

[e]Department of Materials Science and Engineering, University of California, Berkeley, California 94720, United States

[f]School of Materials Science and Engineering, Nanyang Technological University, 50 Nanyang Avenue, Singapore 639798.

ABSTRACT: Zero-dimensional (0D) hybrid organic-inorganic lead halides have been shown to display efficient broadband photoluminescence and are, therefore, of significant interest for artificial lighting applications. However, work that investigates the formability of the materials as a function of templating organic cation structure are rare. This severely limits our ability to rationally design new materials displaying specific structural and photophysical properties. With the goal of accessing rare 0D trimeric bromoplumbates, we have systematically varied templating *N*-alkylpyridinium cations and examined their impact upon inorganic lattice structure. Whereas comparatively short and flexible *N*-alkyl substituents (ethyl, 2-hydroxyethyl, and pentyl) yield one-dimensional (1D) inorganic chains, more rigid substituents (benzyl, acetamidyl, and cyanomethyl) afford hybrids composed of lead-bromide face-sharing trimers ($[Pb_3Br_{12}]^{6-}$). Of the rigid substituents studied, benzyl groups were found to enforce the highest level of distortion of the $[PbBr_6]^{4-}$ octahedra that comprise their trimeric structures. Upon exposure to ultra-violet (UV) light, *N*-benzylpyridinium lead-bromide $(\mathbf{1})_6[Pb_3Br_{12}]$ exhibits a broadband emission, centered at 571 nm, which spans from 400 to 800 nm. More specifically, it displays a large Stokes shift of ca. 1.39 eV and a full width at half maximum (FWHM) of ca. 146 nm. This broadband emission decays with a comparatively long lifetime of 426 ns at room temperature, which increases to 5.8 μs at 77 K. The reduced size and dimensionality of its inorganic lattice also results in a photoluminescence quantum yield (at least 10 %) that is approximately one order magnitude higher than that of its 1D congeners. Mechanistically, broadband emission in $(\mathbf{1})_6[Pb_3Br_{12}]$ is believed to originate from triplet excited state(s) obtained from excited-state structural reorganization of the $[Pb_3Br_{12}]^{6-}$ moiety.

INTRODUCTION

In recent years, organic-inorganic metal halide hybrids have been intensively investigated due to the exceptional versatility of their structural and optoelectronic properties.[1-3] When appropriate organic and inorganic components are chosen, the connectivity of their constituent metal halide polyhedra can be tuned to provide three- (3D), two- (2D), one- (1D), or zero-dimensional (0D) anionic inorganic architectures.[4-9] Such structural variety implies that there is a vast parameter space available for exploration of novel structures that may exhibit new and useful features. For example, lowering the dimensionality of the inorganic lattice leads to more localized electronic states and, consequently, narrower conduction and valence bands. This promotes self-trapping of excitons and yields stronger exciton emission. As a result, unlike the narrow, weakly Stokes-shifted emission bands, typically, observed in 3D metal halide hybrids, 2D, 1D and 0D materials have been shown capable of displaying efficient and heavily Stokes-shifted luminescence, at a wide range of wavelengths.[10-15] Such properties render the low-dimensional materials promising phosphors for artificial illumination.

Structurally, 2D metal halide hybrids can be viewed as being derived from their 3D counterparts by slicing the inorganic lattice along either the (100), (110), or (111) crystallographic planes.[1-3, 16] These 2D structures are typically templated by long, narrow organic cations containing primary ammonium functionality, which permit efficient packing and exhibit strong H-bonding interactions

with the inorganic lattice.[1-3, 16] Although early observations of broadband emission in 2D perovskites were limited to comparatively rare corrugated (110)-oriented structures,[17-18] the more common (100) variants were also later shown to exhibit similar broad PL features, albeit with a strong dependence on temperature.[19-20] The physical origin of the broadband emission in these materials has been attributed to transient self-trapping of excitons in the inorganic lattice, which relax radiatively (to the ground state) from a broad and structurally distorted excited state.[14, 21-22] Although organic-inorganic metal halides are often considered to be similar to inorganic semiconductors, with extended band structures, it has been suggested that exciton self-trapping in these materials involves excited state structural reorganization (distortion and/or bond breaking).[23-24] This results in conversion of delocalized excitons to localized excitons. Alternatively, it has been proposed that permanent color centers, such as positive and negative ion vacancies, and atoms in interstitial sites, are responsible for the observed exciton trapping and luminescence processes.[25]

Meanwhile, inclusion of organic cations containing sterically hindered charge centers can lead to 1D structures, in which the metal-halide octahedra arrange in chains *via* different connectivity modes (face-, corner-, or edge-sharing).[1-3, 6] In addition, 0D hybrids consisting of discrete molecular mono- or oligometallate structures can be obtained with organic cations possessing rigid and/or bulky substituents.[1-4] As a consequence of pronounced structural distortion upon photoexcitation, these materials typically display broadband emissions with large Stokes shifts.[7-8, 26] Furthermore, owing to abundant exciton self-trapping states and enhanced electron-phonon coupling in their organic-inorganic 'host-guest' lattices, highly efficient PL has been demonstrated for 1D and 0D hybrid materials.[11-12, 27-32] In particular, broadband emission with photoluminescence quantum efficiencies (PLQE) of up to 10 – 20 % have been reported for 1D hybrids. Further reducing the dimensionality to 0D clusters was shown to allow for further improvement of the PLQE to near unity values.

As might be inferred from the aforementioned reports, the efficiency of PL emission from metal halide hybrids is highly sensitive to dimensionality of the inorganic lattice and the nature of the templating cations. Thus, any work that contributes to our understanding of the molecular design criteria required for successful formation of 0D structures, which display broadband emission of superior efficiency, is of significant value. Unfortunately, despite the plethora of reports detailing 1D and 0D metal-halide hybrids templated by organic cations of diverse architectures, including those based around hydrocarbon-,[11, 33-35] heteroatom-endowed linear aliphatic,[36-39] cyclic aliphatic,[7, 26, 40-41] and aromatic moieties,[31-32, 42-43] systematic studies of the impact of cation structure upon inorganic lattice structure and PL properties are still relatively scarce.[35, 38, 44] Instead, the overwhelming majority of works involve the use of largely, unrelated organic cations, which make structural analysis difficult. As a result, our ability to rationally dictate the dimensionality of the materials through the modification of organic cations is limited and accessing materials with specific inorganic lattice fine structure is rather hit-and-miss.

Our group is interested in investigating the impact of systematic variation of templating organic cation upon the structure of self-assembled low-dimensionality lead halide inorganic lattices, and its concomitant influence upon their photophysical properties. For instance, we have shown that appending hydrogen bonding functionalities to viologens can induce their dimerization and endow the resulting 1D materials with photoconductivity.[45] In addition, we reported the role of primary ammonium groups ($-NH_3^+$) as a prerequisite for formation of 2D lead-halide perovskites.[46] Neutral (i.e. uncharged) H-bond donor functional groups, such as hydroxyl, carboxyl, and carbonamide were, on the other hand, found to result in formation of 1D structures. We further demonstrated that slight modification in organic cation structure would lead to formation of 2D perovskites with different interoctahedral connectivity that render the materials to exhibit favorable white-light emitting behaviors.[47] The unifying theme across these studies is the use of cyclic cations, such as pyridiniums, with appended alkyl substituents, which are straightforward to structurally vary and prepare.

Utilizing the aforementioned cyclic ammonium cation motifs, we sought to access comparatively rare trimeric bromoplumbate compounds. To this end, a series of *N*-alkylpyridinium salts were prepared and used to template formation of new low dimensional organic-inorganic lead bromide hybrids (**1** – **6**; **Fig. 1**). Based upon literature precedent,[46, 48-49] it was anticipated that inclusion of flexible and short *N*-alkyl substituents, such as ethyl (**4**), pentyl (**5**) and 2-hydroxyethyl (**6**), would result in assembly of 1D inorganic chains. The coulombic interactions between the pyridinium rings and inorganic lattice, in such systems, cause the former to orientate parallel to the latter. These interactions are distinct from those that dominate in 2D perovskites, where H-bonding interactions associated with the ammonium functionality of the cations are a controlling factor.[2, 16, 50] By extension, it was postulated that relatively rigid *N*-alkyl substituents, such as benzyl (**1**), acetamidyl (**2**) and cyanomethyl (**3**), would increase the effective steric impact of the organic cation and, thereby, cause a further reduction of the dimensionality of the bromoplumbate. This proved to be true and allowed synthesis of a handful of rare trimeric bromoplumbates. We performed detailed studies of the optical properties of one of them, $(\mathbf{1})_6[Pb_3Br_{12}]$, and found that it displays heavily Stokes-shifted, broadband emission that is more efficient that it's 1D analogues.

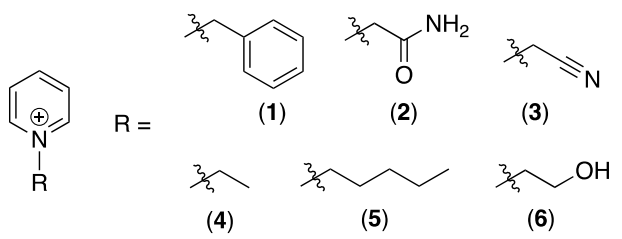

Figure 1. The *N*-alkylpyridinium cations used in this work.

EXPERIMENTAL METHODS

Chemicals. Lead(II) bromide (99.999%), Lead(II) chloride (99.999%), Lead(II) iodide (99.999%), bromoethane (≥99%), 1-bromopentane (98%), 2-bromoethanol (95%), and 2-bromoacetamide (98%) were obtained from Sigma Aldrich, while pyridine (anhydrous, 99.5+%), α-bromotoluene (99%), 2-bromo-acetonitrile (96%), and α-chlorotoluene (99%) were purchased from Alfa Aesar. Unless otherwise stated, all reagents were used without purification.

Synthesis. The following general procedure was used to synthesize the *N*-alkylpyridinium bromide salts: a round bottom flask was charged with pyridine (1 equivalent) and 1.1 equivalent of the requisite bromoalkyl reagent. Acetonitrile was added and resulting mixture was stirred at reflux, under an argon atmosphere, for 1 – 2.5 days. The course of the reaction was monitored using $_1$H NMR spectroscopy and upon completion it was allowed to cool to room temperature. The precipitate obtained was isolated by filtration, washed thoroughly with diethyl ether, and dried *in vacuo* to give the desired products.

1-(benzyl)pyridin-1-ium bromide, (1)Br. Isolated as a brown solid (1.37 g; 90% yield). $_1$H NMR (400 MHz, DMSO-d6): δ 9.36 (d, 2 H, ArH), 8.65 (dd, 1 H, ArH), 8.20 (dd, 2 H, ArH), 7.60 (dd, 2 H, ArH), 7.41 (m, 3 H, ArH), 6.00 (s, 2 H, CH_2). $_{13}$C{$_1$H} NMR (100 MHz, DMSO-d6): δ 146.0, 144.8, 134.3, 129.3, 129.2, 128.8, 128.4, 63.0.

1-(acetamidyl)pyridin-1-ium bromide, (2)Br. Isolated as a white solid (1.11 g; 91% yield). $_1$H NMR (400 MHz, DMSO-d6): δ 8.97 (d, 2 H, ArH), 8.65 (dd, 1 H, ArH), 8.18 (dd, 2 H, ArH), 8.02 (s, 1 H, $C(O)NH_2$), 7.69 (s, 1 H, $C(O)NH_2$), 5.41 (s, 2 H, CH_2). $_{13}$C{$_1$H} NMR (100 MHz, DMSO-d6): δ 166.0, 146.2, 146.0, 127.4, 61.5.

1-(cyanomethyl)pyridin-1-ium bromide, (3)Br. Isolated as a white solid (0.78 g; 83% yield). $_1$H NMR (400 MHz, DMSO-d6): δ 9.16 (d, 2 H, ArH), 8.71 (dd, 1 H, ArH), 8.23 (dd, 2 H, ArH), 5.99 (s, 2 H, CH_2). $_{13}$C{$_1$H} NMR (100 MHz, DMSO-d6): δ 147.6, 145.5, 128.6, 114.3, 47.7.

1-(ethyl)pyridin-1-ium bromide, (4)Br. Isolated as a white solid (1.25 g; 84% yield). $_1$H NMR (400 MHz, DMSO-d6): δ 9.28 (d, 2 H, ArH), 8.63 (dd, 1 H, ArH), 8.17 (dd, 2 H, ArH), 4.72 (q, 2 H, CH_2), 1.52 (t, 3 H, CH_3). $_{13}$C{$_1$H} NMR (100 MHz, DMSO-d6): δ 146.0, 145.2, 128.6, 56.8, 16.9.

1-(pentyl)pyridin-1-ium bromide, (5)Br. Isolated as a yellow solid (1.22 g; 91% yield). $_1$H NMR (400 MHz, DMSO-d6): δ 9.20 (d, 2 H, ArH), 8.63 (dd, 1 H, ArH), 8.18 (dd, 2 H, ArH), 4.66 (t, 2 H, CH_2), 1.92 (m, 2 H, CH_2), 1.33 (m, 4 H, CH_2), 0.85 (t, 3 H, CH_3). $_{13}$C{$_1$H} NMR (100 MHz, DMSO-d6): δ 145.5, 144.7, 127.9, 60.2, 30.4, 27.2, 21.4, 13.5.

1-(2-hydroxyethyl)pyridin-1-ium bromide, (6)Br. Isolated as a brown solid (0.94 g; 88% yield). $_1$H NMR (400 MHz, DMSO-d6): δ 9.09 (d, 2 H, ArH), 8.63 (dd, 1 H, ArH), 8.17 (dd, 2 H, ArH), 4.73 (t, 2 H, CH_2), 3.86 (t, 2 H, CH_2). $_{13}$C{$_1$H} NMR (100 MHz, DMSO-d6): δ 145.7, 145.2, 127.7, 63.1, 60.0.

1-benzylpyridin-1-ium chloride, (1)Cl. Isolated as pale yellow oil (1.12 g; 85% yield). $_1$H NMR (400 MHz, DMSO-d6): δ 9.29 (d, 2 H, ArH), 8.63 (dd, 1 H, ArH), 8.19 (dd, 2 H, ArH), 7.59–7.40 (m, 5 H, ArH), 5.91 (s, 2 H, CH_2). $_{13}$C{$_1$H} NMR (100 MHz, DMSO-d6): δ 146.0, 144.9, 134.3, 129.4, 129.2, 128.8, 128.5, 63.2.

1-benzylpyridin-1-ium iodide, (1)I. Isolated as brown solid (1.17 g; 83% yield). $_1$H NMR (400 MHz, DMSO-d6): δ 9.20 (d, 2 H, ArH), 8.64 (dd, 1 H, ArH), 8.19 (dd, 2 H, ArH), 7.58–7.38 (m, 5 H, ArH), 5.88 (s, 2 H, CH_2). $_{13}$C{$_1$H} NMR (100 MHz, DMSO-d6): δ 146.0, 144.8, 134.3, 129.4, 129.2, 128.8, 128.5, 63.3.

Crystal growth. In general, vials were charged with concentrated solutions (~0.25 – 0.33 M) of stoichiometric amounts of $PbBr_2$ and *N*-alkylpyridinium halide salt in dimethyl sulfoxide (DMSO), after which the antisolvent acetone was introduced by the vapor diffusion method, under ambient conditions. The single crystals, which formed within 2 – 7 days (~37-72% yield based on Pb content), were either used in X-ray crystallographic studies or isolated and dried *in vacuo* for further characterization.

Nuclear Magnetic Resonance (NMR) spectroscopy. $_1$H and $_{13}$C{$_1$H} NMR spectra of organic compounds were recorded in DMSO-d6 solution using a Bruker AV400 spectrometer. Chemical shift values (ppm) are referenced against residual protic solvent peaks.

X-ray crystallography. Crystals were mounted on a Bruker X8 Quest CPAD area detector diffractometer and data was collected using a IμS 3.0 Microfocus Mo-Kα radiation source (λ = 0.71073 Å), at cryogenic temperatures (100 K). Data reduction and absorption corrections were performed using the SAINT and SADABS software packages, respectively.[51] All structures were solved by direct methods and refined by full-matrix least squares procedures on F_2, using the Bruker SHELXTL-2014 software package.[52-53] Non-hydrogen atoms were anisotropically refined, after which hydrogen atoms were introduced at calculated positions and the data was further refined. The graphical illustrations of crystal structures used throughout the main paper and supporting information were created using the program VESTA.[54]

Powder X-ray diffraction. Powder X-ray diffraction measurements were conducted using a Bruker AXS D8 ADVANCE system containing a Cu Kα radiation source (λ = 1.5418 Å). The XRD spectra were recorded with an incident angle of 5°, a step size of 0.05°, and a delay time of 1s for each step.

Density Functional Theory (DFT) Calculations. First-principles DFT calculations were performed to investigate the electronic structure of the compound (**1**)$_6$[Pb_3Br_{12}]. Calculations considered a 495-atom unit cell with atomic positions taken from the refined experimental structure, without further optimization. DFT calculations were performed using version 5.4.4 of the Vienna Ab initio Simulation Package (VASP),[55] employing the Perdew-Burke-Ernzerhof (PBE) Generalized Gradient Approximation (GGA)[56] exchange-correlation functional, with explicit inclusion of spin-orbit-coupling terms employing the approach implemented in VASP. The electron-ion interactions were described with the projector-augmented-wave (PAW)[57] method as implemented in VASP.[58] PAW potentials labeled "PAW_PBE C 08Apr2002", "PAW_PBE N 08Apr2002", "PAW_PBE H

15Jun2001", "PAW_PBE Pb 08Apr2002", and "PAW_PBE Br 06Sep2000" were employed for C, N, H, Pb and Br, respectively. A plane wave cutoff energy of 440 eV was used for the expansion of wavefunctions. For Density of States (DOS) calculations, the tetrahedron method with Blöchl corrections[59] was used and the Brillouin zone was sampled on a kpoint mesh of 2 × 2 × 2. The electronic band structure was evaluated along the special k-point paths in the Brilllouin zone.

UV-vis spectroscopy. UV-vis spectra of polycrystalline samples were collected using a Shimadzu UV-3600 UV-VIS-NIR Spectrophotometer, with $BaSO_4$ as the 100% reflectance reference. The measurements were conducted over a 300 – 800 nm wavelength range, in the diffuse reflectance mode, using an integrating sphere, and a scanning resolution of 0.5 nm s^{-1}. Relative absorbance was obtained from Kubelka–Munk transformation of the reflectance spectra: $\alpha/S = (1 - R)^2(2R)^{-1}$, where R is the reflectance, and α and S are the absorption and scattering coefficients, respectively.

Steady-state, time-resolved, temperature- and power-dependent photoluminescence (PL) spectroscopies. Samples were photoexcited with 325 nm femtosecond laser pulses, generated using an optical parametric amplifier (OPA, Coherent OPerA Solo). The OPA was powered by a Coherent LIBRA laser, with a fundamental wavelength of 800 nm and output pulse-width of ~50 fs, at a repetition rate of 1 kHz. The PL signal was collected using a

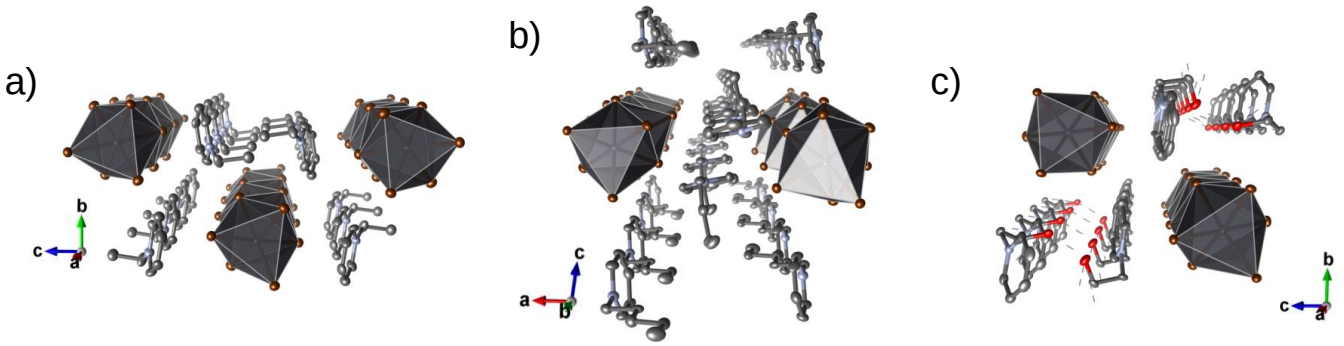

Figure 2. Single crystal X-ray structures of the 1D lead bromide hybrids a) **4**[$PbBr_3$], b) **5**[$PbBr_3$] and c) **6**[$PbBr_3$]. Dark gray, brown, gray, blue and red spheroids represent Pb, Br, C, N and O atoms, respectively. H atoms are omitted for clarity. Thermal ellipsoids are shown at 50% probability.

lens pair and sent to a spectrometer (Princeton Instrument, SP-2500 series), where it was detected by a CCD camera (Pixis-400) or a streak camera (Optronis) in steady-state and TRPL measurements, respectively. The power-dependent measurements were obtained in this configuration by changing the excitation power in the range of 2.5 – 40 μW, using a set of variable density filters. For temperature-dependent studies, the samples were mounted onto a liquid nitrogen-cooled Janis st-300 cryostat, adjusted to the optical plane of the inverted microscope, and measured within the temperature range 77 – 293 K.

Photoluminescence quantum yield. Samples were photoexcited with 325 nm femtosecond laser pulses, generated using an optical parametric amplifier (OPA, Coherent OPerA Solo). The OPA was powered by a Coherent LIBRA laser, with a fundamental wavelength of 800 nm and output pulse-width of ~50 fs, at a repetition rate of 1 kHz and 2.5 μW.

Raman spectroscopy. Raman scattering measurements were performed using a WITec alpha 300RAS confocal Raman microscope. An Acton spectrometer with a diffraction grating of 1800 grooves mm^{-1} (1.3 cm^{-1} resolution) and a thermoelectrically cooled Andor CCD detector were used to collect data. To avoid absorption by the samples, which could lead to photoluminescence and degradation, the 633 nm (red) line from a He–Ne gas laser with a power of 5 mW was chosen, while the laser spot

area was ~1 μm^2. The backscattered Raman signal passed through two 633 nm BragGrate Notch Filters (BNF). Measurements at 80 K were conducted under a nitrogen gas flow cryostat.

RESULTS AND DISCUSSION

X-ray crystal structures of the *N*-alkylpyridinium-templated compounds containing 1D bromoplumbate chains and trimeric bromoplumbates are shown in **Figures 2** and **3**, respectively. (Selected bond lengths are provided in Table 1, and more extensive lists of structural parameters, plus crystallographic and refinement data, are provided in the Supporting Information.) As anticipated, employing flexible *N*-alkyl substituents leads to formation of 1D polymeric chains of the monomer $[PbBr_3]^-$. This is exemplified by the cation *N*-ethylpyridinium (**4**), where the 1D chains in **4**$[PbBr_3]$ (**Figure 2a**) are built from face-sharing of its constituent $[PbBr_6]^{4-}$ octahedra. The coordination sphere of Pb is distorted, with large differences between the lengths of Pb–Br bonds (ranging from 2.8185(13) to 3.3633(13) Å) mutually *trans* to one another along two of the three molecular axes. Despite the potential existence of several C-H···Br intermolecular interactions between the bromoplumbate chains and pyridinium cations, the main driving force for crystal packing is likely to be Coulombic interactions. This notion is supported by the tendency of the pyridinium rings to align parallel to the inorganic lattices, which minimizes separation of the opposing charges of these two components. Furthermore, the structures of **5**$[PbBr_3]$ and **6**$[PbBr_3]$ (**Figs. 2b** and **2c**), whose cations contain pentyl and 2-hydroxyethyl substituents, respectively, show similar properties. This suggests that long-chain linear *N*-alkyl substituents and those with neutral H-bond donor functionality, do not interfere with self-assembly of the 1D Pb-Br polymeric chains.

Table 1. List of selected bond lengths (Å) from the single crystal X-ray structures of $(\mathbf{1})_6[Pb_3Br_{12}]$, $(\mathbf{2})_6[Pb_3Br_{12}]$, $(\mathbf{3})_6[Pb_3Br_{12}]$, **4**$[PbBr_3]$, **5**$[PbBr_3]$, and **6**$[PbBr_3]$.

Compounds	Pb–(μ_2-Br) $^{\alpha}$	Pb–Br$_t$ $^{\beta}$	Pb–Pb
$(\mathbf{1})_6[Pb_3Br_{12}]$	3.0016(4), 3.1665(5)	2.9219(5)	3.9345(5)
$(\mathbf{2})_6[Pb_3Br_{12}]$	3.0583(4), 3.2722(6)	2.8764(4)	3.8458(5)
$(\mathbf{3})_6[Pb_3Br_{12}]$	2.9746(16) - 3.2225(17)	2.8423(17) - 2.9678(16)	3.8143(10) - 3.9365(10)
4$[PbBr_3]$	2.8185(12) - 3.3633(12)		3.9456(16)
5$[PbBr_3]$	2.9895(8) - 3.3423(11)	2.7861(8)	3.9797(5)
6$[PbBr_3]$	2.8874(9) - 3.2526(12)		3.8667(7) - 3.9275(7)

$^{\alpha}$bridging Pb–Br bond lengths. $^{\beta}$Terminal Pb–Br bond lengths.

In contrast, distinct bromoplumbate architectures are obtained with the more rigid substituents of **1**, **2**, and **3** (**Figure 3**), using the same crystallization conditions. More specifically, the resulting

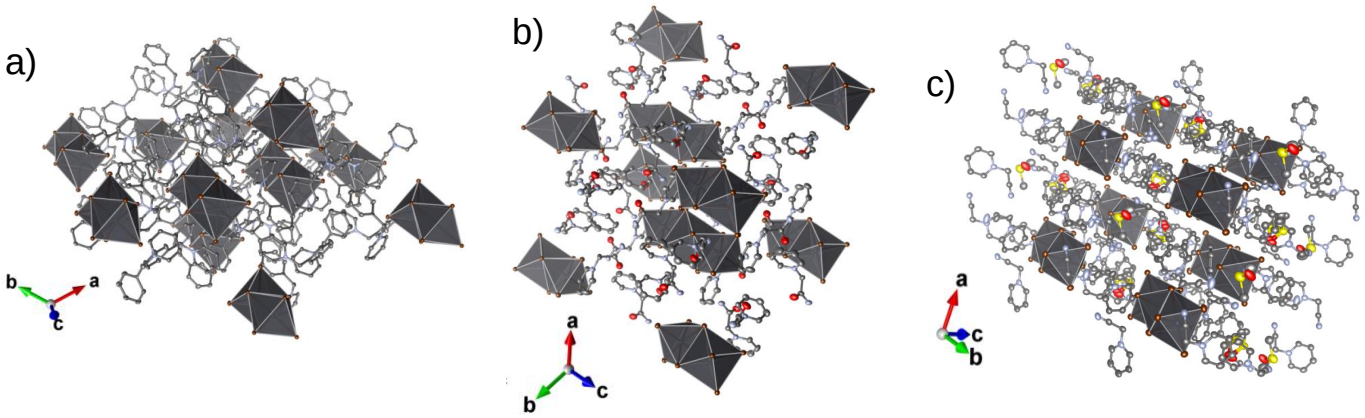

Figure 3. Single crystal X-ray structures of trimeric lead-bromide hybrids a) (**1**)$_6$[Pb$_3$Br$_{12}$], b) (**2**)$_6$[Pb$_3$Br$_{12}$] and c) (**3**)$_6$[Pb$_3$Br$_{12}$]. Dark gray, brown, gray, blue, red, and yellow spheroids represent Pb, Br, C, N, O and S atoms, respectively. H atoms are omitted for clarity. Thermal ellipsoids are shown at 50% probability.

hybrids (**1**)$_6$[Pb$_3$Br$_{12}$], (**2**)$_6$[Pb$_3$Br$_{12}$] and (**3**)$_6$[Pb$_3$Br$_{12}$] are comprised of discrete molecular [Pb$_3$Br$_{12}$]$_{6-}$ trimers that are separated by, and appear at regular intervals in, a matrix of organic countercations. Such inorganic motifs are very rare, relative to 1D and 2D hybrids, and are distinct from the more common 0D compounds composed of monomeric halides.[7, 12, 26-27] In fact, we are aware of only four compounds containing trimeric Pb-Br units.[5, 60-62] The major difference between cations **1** – **3** and **4** – **6**, used in this study, is that the *N*-alkyl substituents in the former group contain sp or sp$_2$ hybridized C atoms. This endows them with a degree of rigidity that inhibits ideal packing around the inorganic octahedra and, thereby, prevents assembly of infinite 1D [PbBr$_3$]$_-$ chains.

The trimers are built from monomeric lead bromide octahedra that link to one another in a face-sharing fashion. As such, all 6 bromide ions in the central [PbBr$_6$]$_{4-}$ octahedra are bridging (μ_2-Br$_-$), whereas the outer [PbBr$_6$]$_{4-}$ octahedra have 3 terminally bound ions (Br$_{t-}$) and 3 that bridge to the central Pb ion. Consistent with expectations, the Pb-Br$_t$ bonds are generally shorter than the Pb–(μ_2-Br) bonds (**Table 1**; for more complete data, see the tables in the Supporting Information). For instance, in (**1**)$_6$[Pb$_3$Br$_{12}$] the former are 2.9219(5) Å long, whereas the latter vary from 3.0016(4) – 3.1665(5) Å. Furthermore, the Pb–(μ_2-Br) distances in the trimers are, on the whole, longer than those in the 1D chains templated by **4**$_+$, **5**$_+$ and **6**$_+$. Notably, there is deviation in the average Pb–Pb distances amongst the three trimers, with those of (**1**)$_6$[Pb$_3$Br$_{12}$] and (**2**)$_6$[Pb$_3$Br$_{12}$] being the longest and shortest, respectively, at 3.9345(5) and 3.8458(5) Å. Although there is some overlap in their ranges, the Pb-Pb separations in the 1D chains are generally longer than those in the bromoplumbate trimers (**Table 1**).

Interestingly, the tendency to form inorganic trimers, rather than 1D structures, is also influenced by the identity of the halide. Whereas replacement of the bromide ions in (**1**)$_6$[Pb$_3$Br$_{12}$] with chloride provides the isostructural, trimer-containing compound (**1**)$_6$[Pb$_3$Cl$_{12}$], combination of PbI$_2$ with (**1**)I affords the 1D iodoplumbate **1**[PbI$_3$] (**Figure S1**). The larger Pb-halide voids formed by the bigger iodide anions are, presumably, better able to accommodate close packing with the *N*-benzylpyridinium cation.

The breaking of 1D bromoplumbate chains into trimeric units is readily apparent in single crystal, low-frequency Raman measurements (**Figure S2**). Based upon a close similarity to vibrations (at 142 cm^{-1}) in published 1D bromoplumbate compounds possessing face-sharing linkages,[6, 63] the vibration in **4**[PbBr$_3$] at 143 cm^{-1} can be assigned as symmetric stretching of comparatively strong Pb–Br bonds. In (**1**)$_6$[Pb$_3$Br$_{12}$], this Raman mode shifts to lower energy (132 cm^{-1}) and decreases in intensity by a factor of ~3. The former indicates weakening of the Pb–Br bonds and an increase in Pb–Br bond lengths, while the latter reflects a decrease of the overall rigidity of bonding. These results are consistent with their X-ray crystal structures, wherein (**1**)$_6$[Pb$_3$Br$_{12}$] contains six terminally-bound halides in each of their trimeric inorganic components, while **4**[PbBr$_3$] has none (i.e., all are bridging). The peaks below 100 cm^{-1}, contributed by vibrations involving scissoring modes of Pb–Br–Pb and Br–Pb–Br, differ as well. However, precise assignment of these features is not straightforward due to the large number of overlapping vibrational modes in this region. As such, exact assignments would require a combination of calculations and measurements at low temperatures.

Overall, the bulky *N*-benzylpyridium cations in (**1**)$_6$[Pb$_3$Br$_{12}$] impose greater structural distortion of their constituent [PbBr$_6$]$_{4-}$ octahedra than the cations that template the other trimeric structures, (**2**)$_6$[Pb$_3$Br$_{12}$] and (**3**)$_6$[Pb$_3$Br$_{12}$] (**Table 2**). The degree of intra-octahedral distortion is assessed via the parameters octahedral elongation (λ_{oct}), octahedral angle variance (σ^2_{oct}), and octahedral bond length distortion (Δ_{oct}),[23, 64] which are calculated using the following equations:

$$\lambda_{oct} = \frac{1}{6}\sum_{i=1}^{6}\left[\frac{d_i}{d_0}\right]^2 \qquad (1)$$

$$\sigma^2{}_{oct} = \frac{1}{11}\sum_{i=1}^{12}(\alpha_i - 90)^2 \qquad (2)$$

$$\Delta_{oct} = \frac{1}{6}\sum_{i=1}^{6}\left[\frac{d_i - d_m}{d_m}\right]^2 \qquad (3)$$

where d_i corresponds to Pb–Br bond length, d_0 to center-to-vertex distance of a regular octahedron of the same volume, d_m to average

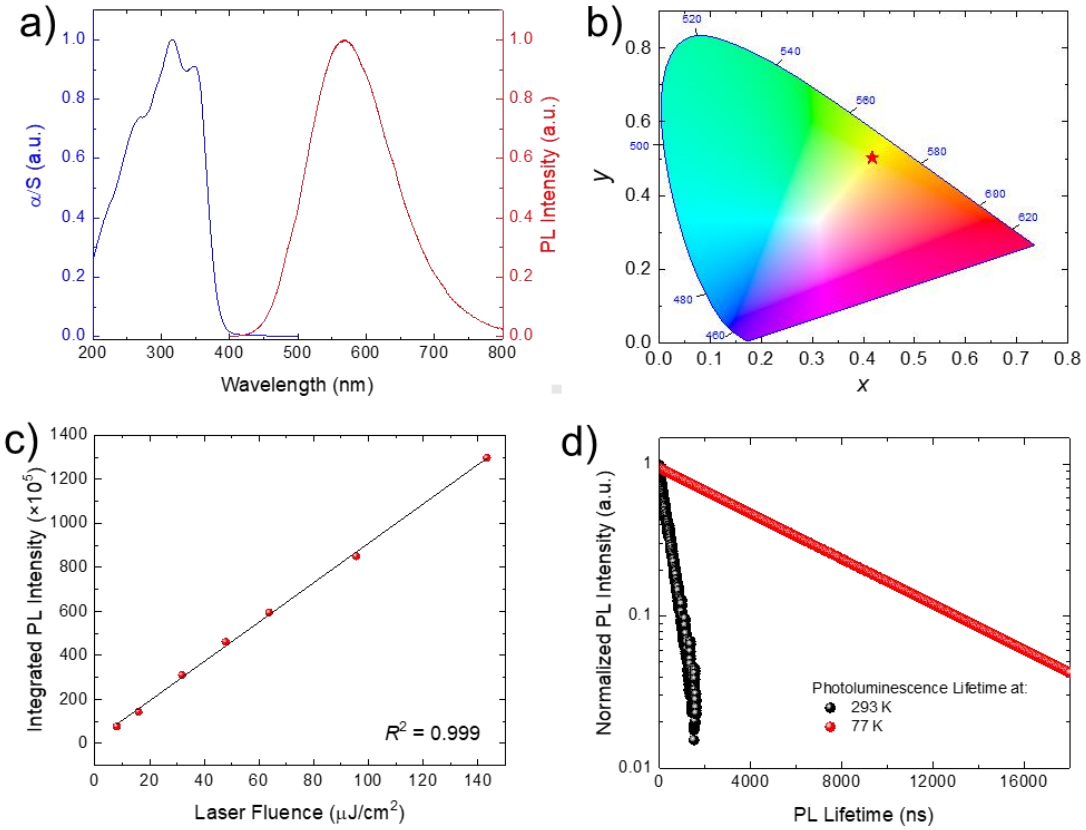

Figure 4 a) Room temperature UV-vis diffuse reflectance spectrum (DRS), transformed using the Kubelka-Munk (K-M) function, and photoluminescence (PL, λ_{ex} = 350 nm) spectrum of (**1**)$_6$[Pb$_3$Br$_{12}$]. b) Chromaticity coordinates for the PL emission of (**1**)$_6$[Pb$_3$Br$_{12}$]. c) Laser fluence-dependent integrated PL intensity of (**1**)$_6$[Pb$_3$Br$_{12}$], recorded at 293 K in the range 8 – 143 μJ /cm$_2$, plus a linear fit of the data. d) Time-resolved PL spectra of (**1**)$_6$[Pb$_3$Br$_{12}$], recorded at an emission wavelength of 570 nm, at temperatures of 77 and 293 K.

bond length, and α_i to individual Br–Pb–Br angle. λ_{oct} and σ_{2oct} provide a quantitative measure of octahedral distortion independent of the effective size of the octahedron, with larger values equating to greater distortion.

It was previously reported, and is generally accepted, that the tendency of 2D bromoplumbate perovskites to demonstrate broadband photoluminescence increases with increasing distortion of their constituent lead bromide octahedra.[6, 65] Thus, it is noteworthy that the levels of intra-octahedral structural distortion displayed by (**1**)$_6$[Pb$_3$Br$_{12}$] – (**3**)$_6$[Pb$_3$Br$_{12}$] are very large, even relative to broadband-emitting 2D perovskites.[65-67] This is a direct consequence of the very different coordination spheres of the "central" and two "terminal" lead ions that comprise the trimers. More specifically, the terminal [PbBr$_6$]$_{4-}$ octahedra contain 3 terminally-bound Br$_-$ ions and a further three that μ_2-bridge in a facial fashion to a central Pb$_{2+}$ ion. By extension, the central Pb$_{2+}$ ions are coordinated only to bridging Br$_-$ ions. The inherently lower symmetry of the coordination sphere of the terminal Pb$_{2+}$ ions, combined with the significant difference between the bond lengths and angles to μ_2-bridging Br$_-$ ions versus terminally-bound Br$_-$ ions, results in the aforementioned large deviations from ideal octahedral symmetry. Consistent with our expectations, all of the trimeric hybrids reported herein were found to exhibit broadband emission (**Figure S3**). Of these, we elected to study the optical properties of the compound displaying the largest intra-octahedral distortions, (**1**)$_6$[Pb$_3$Br$_{12}$], in greater detail.

Table 2. Distortion parameters derived from the single crystal X-ray structures of the trimeric bromoplumbates (**1**)$_6$[Pb$_3$Br$_{12}$], (**2**)$_6$[Pb$_3$Br$_{12}$], and (**3**)$_6$[Pb$_3$Br$_{12}$]$_a$

Compound	λ_{oct} (avg)$_b$	σ_{2oct} (avg)$_c$	Δ_{oct} (×10$_{-4}$)$_d$

(**1**)$_6$[Pb$_3$Br$_{12}$]	1.012	39.07	10.79
(**2**)$_6$[Pb$_3$Br$_{12}$]	1.005	13.04	27.66
(**3**)$_6$[Pb$_3$Br$_{12}$]	1.011	31.93	21.93

[a]Averaged distortion parameters are given because the unit cells of (**1**)$_6$[Pb$_3$Br$_{12}$], (**2**)$_6$[Pb$_3$Br$_{12}$] and (**3**)$_6$[Pb$_3$Br$_{12}$] contain two, two, and three geometrically distinct octahedra, respectively. Further details are provided in the SI. [b]Octahedral elongation. [c]Octahedral angle variance. [d]Octahedral bond length distortion.

Single crystals of (**1**)$_6$[Pb$_3$Br$_{12}$] appear colorless and transparent under ambient light, which is indicative of little-to-no light absorption in the visible region and a large HOMO-LUMO energy gap. Consistent with this, its pseudoabsorption spectrum, converted from diffuse-reflectance measurements using the Kubelka–Munk function, shows an absorption band with a maxima of 318 nm (**Figure 4a**). Upon photoexcitation by ≤ 375 nm UV light, (**1**)$_6$[Pb$_3$Br$_{12}$] exhibits strong photoluminescence (PL) at room temperature. The emission band is broad, with a maxima at 571 nm, an emission width of ca. 1.45 eV, and a full width at half maximum (FWHM) of ca. 146 nm (**Figure 4a**). Relative to its absorption onset, the observed PL exhibits a large Stokes shift of ca. 1.39 eV.

A similar PL feature was also observed in ball-milled powder samples of (**1**)$_6$[Pb$_3$Br$_{12}$] (**Figure S4**), which indicates that differences in particle size and defects do not significantly affect the emission. (Purity of the bulk (**1**)$_6$[Pb$_3$Br$_{12}$] was confirmed using powder X-ray diffraction, shown in **Figure S5**, where the obtained pattern exhibits a near perfect match with the simulated XRD pattern.) The observed broadband emission corresponds to "warm" white-light, with a correlated colour temperature (CCT) of 3667 K, Commission Internationale de l'Eclairage (CIE) chromaticity coordinate (0.43; 0.50), and colour rendering index (CRI) of 64 (**Figures 4b**), making it suitable for indoor illumination.

The PLQE of (**1**)$_6$[Pb$_3$Br$_{12}$] was determined to be at least 10 % (**Figure S6**), which is similar to that reported for other trimeric bromoplumbates.[29] As a frame of reference, the prototypical 1D compound **4**[PbBr$_3$] exhibits a PLQE of ca. 1.0 %, which is of a similar magnitude to values reported for other 1D lead-bromide hybrids (0.4 – 0.6 %).[6, 44] Thus, although the 1D materials templated by **4** – **6** also exhibit broadband emission (**Figure S7**), moving to a 0D trimer can yield a ten-fold enhancement of PLQE. This is a straightforward consequence of increased quantum-confinement and illustrates why a decrease in dimensionality is advantageous.

Identical PL features were obtained for (**1**)$_6$[Pb$_3$Br$_{12}$] when excitation wavelengths shorter than 375 nm were used (**Figure S8**). Such invariance suggests that the broadband emission is an intrinsic feature of this material. In addition, photoluminescence excitation (PLE) spectra probing the emission band over the range 450 – 700 nm retain the same shape and features (**Figure S9**). This implies that the entirety of the observed emission originates from a common set of excited states. Moreover, the PLE spectra exhibit similar onsets of ca. 390–400 nm as the UV-vis data, which further evidences the intrinsic origin of the broadband PL. This conclusion is also supported by power-dependent continuous-wave PL measurements. If the emission arose from permanent defects, PL would be expected to saturate as these traps become filled. Instead, PL intensity is found to increase linearly with fluence from 8 to 143 μJ cm^{-2} at 293 K (**Figures 4c and S10**), with no signs of saturation. Also, no blue-shift of PL spectra was observed with increasing excitation fluence, ruling out the possibility of it being deep-trap emission.

The luminescent decay of (**1**)$_6$[Pb$_3$Br$_{12}$] at room temperature was recorded and, as shown in **Figure 4d**, monoexponential fitting of its broadband emission gives a comparatively long lifetime of approximately 426 ns. Additionally, no significant variation of PL lifetime is seen across different emission wavelengths (**Figure S11**). Decrease of the temperature to 77 K results in an increase the luminescent decay lifetime to around 5.8 μs (also by single-exponential fitting). This is similar to observations reported for 0D organic-inorganic metal halide hybrids that have emissions from excitons localized in individual metal halide clusters.[26-27, 68] In particular, the aforementioned behavior of (**1**)$_6$[Pb$_3$Br$_{12}$] is indicative of emission originating from a triplet excited state(s), similar to the phosphorescence commonly associated with heavy metal complexes.[69]

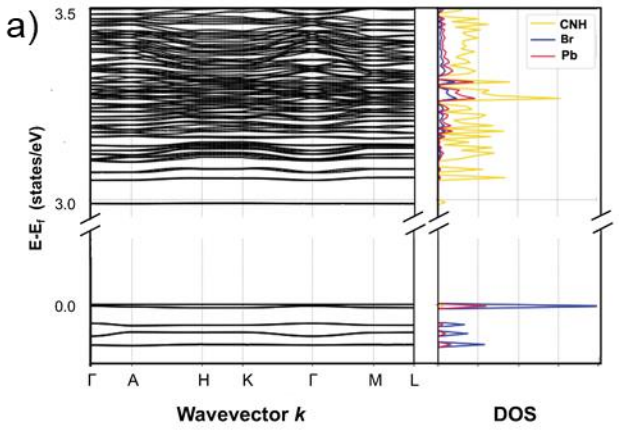

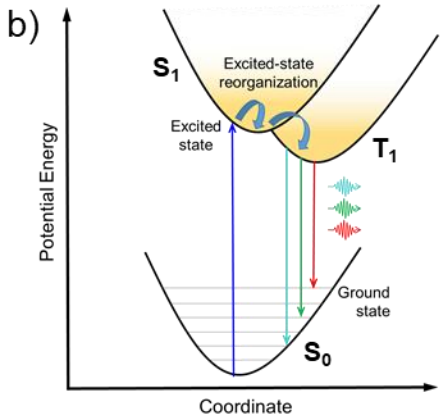

Figure 5. a) Density Functional Theory (DFT) calculated electronic band structure and density of states (DOS) plots for (**1**)$_6$[Pb$_3$Br$_{12}$]. The computational methodology employed is described above. b) Schematic depiction of the proposed mechanism of broadband emission in (**1**)$_6$[Pb$_3$Br$_{12}$]. The straight and curved arrows represent optical transitions and excited state rearrangement, respectively.

Upon lowering the temperature to 77 K, the emission spectrum of (**1**)$_6$[Pb$_3$Br$_{12}$] becomes progressively narrower and shifts slightly to higher energy (**Figures S12 and 13**). This, presumably, reflects reduced thermal population of higher vibrational states at low temperatures. Interestingly, we did not observe additional bands appearing in the PL spectrum within the temperature range of 77 – 293 K. This is in contrast to the previously reported trimeric Pb-Br compound templated by the 1-butyl-1-methylpyrrolidinium cation, (**bmpy**)$_6$[Pb$_3$Br$_{12}$],[70] which was shown to exhibit two emission peaks, at 501 and 564 nm, with respective decay lifetimes of 18 and 44 μs, at 77 K. To explain this phenomenon, the presence of two co-existing excited-state energy minima, accessed with different energy barriers, was proposed. The origin of the difference between the PL behaviour of (**1**)$_6$[Pb$_3$Br$_{12}$] and other Pb-Br trimers is not clear at this stage, and the in-depth photophysics investigations that would be required to elucidate the mechanism of emission are beyond the scope of the current work. However, we suspect that it stems from different structural distortions in the photoexcited state(s) that are themselves the result of differences in the supramolecular interactions between the inorganic clusters and the accompanying templating organic cations.

Modelling the temperature dependence (77 – 293 K) of the integrated PL intensity and decay lifetime of (**1**)$_6$[Pb$_3$Br$_{12}$] with the Self-Trapped Exciton (STE) Model, which is normally applied to typical semiconducting materials, yields good fits (**Figures S14 and S15**).[43, 71] However, unlike hybrid metal halide systems of higher dimensionalities,[14, 21] (**1**)$_6$[Pb$_3$Br$_{12}$] is not an extended solid; it is comprised of discrete molecular entities. Consistent with this, its DFT calculated electronic structure exhibits nearly dispersionless "bands" (**Figure 5a**). This implies that the photogenerated excitons would be very much localized in the individual bromoplumbate clusters, as they are spacially isolated from one another and have no appreciable electronic coupling. As such, the highly Stokes shifted broadband emission observed in (**1**)$_6$[Pb$_3$Br$_{12}$] can be assumed to a result of structural reorganization of the photoexcited trimers.[72-75]

A further question is whether the observed PL behaviour is a consequence of energy/charge transfer from the Pb-Br trimers to the organic countercations, with broadband emission from the latter. Accordingly, the UV-vis DRS of (**1**)Br was recorded (Figure S17), and it was found to exhibit an extremely weak feature at similar energies to the broadband emission of (**1**)$_6$[Pb$_3$Br$_{12}$]. Furthermore, the DFT calculations yielded two sets of largely cation-based bands (not shown), at 1.36-1.68 and 2.24-2.59 eV above the Fermi level, intermediate between the Pb and Br dominated highest occupied molecular orbitals (HOMOs) and lowest unoccupied molecular orbitals (LUMOs), which are respectively within 0.5 eV of the Fermi level and approximately 3 – 3.5 eV above the Fermi level. However, given the spatial separation of the organic and inorganic components, which results in the majority of Pb 6s and Br 4p contributions to the HOMOs being from within the same trimer, there is likely to be significant barriers to energy transfer between them. Considering this and the relatively high intensity and long lifetimes of broadband emission of (**1**)$_6$[Pb$_3$Br$_{12}$], we favour retention of the exciton within the [Pb$_3$Br$_{12}$]$_{6-}$ moiety. Analogous (and well-evidenced) conclusions were drawn for the 0D tetraphenylphosphonium-templated chloroantimonate (**Ph$_4$P**)$_2$[SbCl$_5$], which displays similar broadband white light emission properties.[12] DFT calculations for this compound similarly gave organic cation-based LUMOs, but they also showed that the excited triplet state of the SbCl$_{5-}$ moiety was substantially stabilized and the calculated emission from this state was in excellent agreement with experiment.

A schematic depiction of our proposed broadband emission mechanism is provided in **Figure 5b**. Upon photon absorption, the [Pb$_3$Br$_{12}$]$_{6-}$ species are initially excited to a high energy singlet excited state. Subsequently, there is ultrafast excited state structural reorganization and intersystem crossing to lower energy triplet excited state(s), from which the highly Stokes-shifted broadband emission occurs. This general mechanism has been demonstrated (and is widely accepted) for heavy atom-containing metal complexes and molecules,[71-72, 74-75] and has been recently proposed for similar 0D Pb-, Sn-, Ge-, and Sb-based hybrids.[7, 12, 68] Although it has not yet been confirmed that a triplet exciton can be accessed and stabilized by the Pb-Br trimers of (**1**)$_6$[Pb$_3$Br$_{12}$], its relatively long emission lifetime (**Figure 4d**) is consistent with this assumption. Future studies may clarify these points.

One of the most important factors for assessing the applicability of a material for practical lighting applications, is its stability upon storage and exposure to light, under ambient conditions. Accordingly, we measured the PL spectrum of (**1**)$_6$[Pb$_3$Br$_{12}$] after storage in air, with a relative humidity (RH) of 70 %, at room temperature (RT) for 3 and 6 months. As shown in **Figure 6a**, virtually no change in PL emission shape and position was observed. In addition, upon continuous excitation by 350 nm wavelength light (5 μJ cm^{-2} fluence, at a 1 kHz repetition rate) for approximately six hours, under ambient conditions (RH = 70 %, RT), (**1**)$_6$[Pb$_3$Br$_{12}$] was able to retain around 90% of its initial PL intensity (**Figure 6b**). These measurements indicate relatively good stability. We attribute this to the presence of the bulky *N*-benzylpyridinium cations, which acts as a protective "matrix" or "host" for the "guest" [Pb$_3$Br$_{12}$]$_{6-}$ moieties.

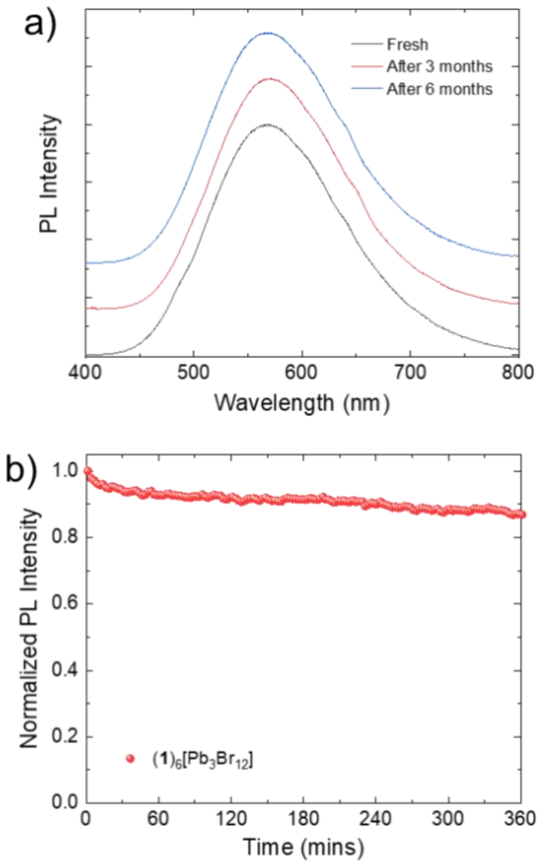

Figure 6. a) Photoluminescence (PL, λ_{ex} = 350 nm) spectra of (**1**)$_6$[Pb$_3$Br$_{12}$] recorded fresh and after storage for 3 and 6 months under ambient conditions (room temperature (RT) and relative humidity (RH) = 70 %). b) Normalized PL intensity of (**1**)$_6$[Pb$_3$Br$_{12}$] under constant illumination, using an excitation wavelength of 350 nm and a laser fluence of ~5 μJ cm^{-2}, under ambient conditions (RT and RH = 70 %).

CONCLUSIONS

In summary, we set out to selectively induce formation of trimeric bromoplumbates by engineering the molecular structure of templating pyridinium cations. This was successfully achieved through incorporation of comparatively rigid benzyl, acetamidyl, and cyanomethyl substituents, which contain sp^2 or sp hybridized C atoms. The resulting "0D" [Pb$_3$Br$_{12}$]$^{6-}$ trimers are very rare and we aware of only four examples having been published prior to this study. As such, we have almost doubled the number known. Of the three trimers detailed herein, the *N*-benzylpyridinium containing compound (**1**)$_6$[Pb$_3$Br$_{12}$] exhibits the most severe distortions of the constituent lead-bromide octahedra (i.e., coordination spheres). It's highly confined inorganic lattice and strong intra-octahedral distortions result in PL emission that is efficient (at least 10% PLQE), relative to its 1D congeners, ultra-broad (ca. 146 nm), and highly Stokes-shifted (1.39 eV). Mechanistically, the broadband emission is deduced to proceed via excited-state structural reorganization of the inorganic [Pb$_3$Br$_{12}$]$^{6-}$ to an emissive triplet state(s). Further studies are required to confirm this assertion and exclude the possibility of energy/charge transfer to (and emission from) the organic cation. Regardless, our work demonstrates deliberate tailoring of the Pb-halide lattice structure at a molecular level in order to induce desirable photophysical properties. This represents a rare example of rational design of the microscopic structure of haloplumbates, and the cation-inorganic lattice structure correlations elucidated herein can be used to inform future engineering of p-block metal halide materials possessing specific motifs and dimensionalities.

AUTHOR INFORMATION

Corresponding Author

*E-mail: jengland@ntu.edu.sg.

*Email: nripan@ntu.edu.sg.

Notes

The authors declare no competing financial interest. CIF data for associated crystal structures have been deposited in the Cambridge Crystallographic Data Centre under deposition numbers CCDC 1915772-1915779.

ACKNOWLEDGMENT

JE thanks NTU for funding (M4081442). NM, KTM, BF would like to acknowledge the funding from the Singapore National Research Foundation through the Singapore–Berkeley Research Initiative for Sustainable Energy (SinBeRISE) CREATE Program, Office of Naval Research Global (ONRG-NICOP-N62909-17-1-2155), and the Competitive Research Program: NRF–CRP14–2014–03. TCS and DG acknowledge the support from the Ministry of Education Tier 2 grants MOE2017-T2-1-001 and MOE2017-T2-2-002 and from the Singapore National Research Foundation through the NRF Investigatorship (NRF-NRFI-2018-04). The efforts of S.S. and M.A., associated with the DFT calculations were funded by the U.S. Department of Energy, Office of Science, Office of Basic Energy Sciences, Materials Sciences and Engineering Division under Contract No. DE-AC02-05-CH11231 (Materials Project program KC23MP). The computations made use of resources at the National Energy Research Scientific Computing Center (NERSC), a U.S. Department of Energy Office of Science User Facility operated under Contract No. DE-AC02-05CH11231.

REFERENCES

1. Manser, J. S.; Christians, J. A.; Kamat, P. V., Intriguing Optoelectronic Properties of Metal Halide Perovskites. *Chem. Rev.* **2016,** *116* (21), 12956–13008.
2. Saparov, B.; Mitzi, D. B., Organic-Inorganic Perovskites: Structural Versatility for Functional Materials Design. *Chem. Rev.* **2016,** *116* (7), 4558–4596.
3. Lin, H.; Zhou, C.; Tian, Y.; Siegrist, T.; Ma, B., Low-Dimensional Organometal Halide Perovskites. *ACS Energy Lett.* **2017,** *3* (1), 54–62.
4. Mercier, N.; Louvain, N.; Bi, W., Structural diversity and retro-crystal engineering analysis of iodometalate hybrids. *CrystEngComm* **2009,** *11* (5).

5. Smith, M. D.; Watson, B. L.; Dauskardt, R. H.; Karunadasa, H. I., Broadband Emission with a Massive Stokes Shift from Sulfonium Pb–Br Hybrids. *Chem. Mater.* **2017,** *29* (17), 7083–7087.
6. Mao, L.; Guo, P.; Kepenekian, M.; Hadar, I.; Katan, C.; Even, J.; Schaller, R. D.; Stoumpos, C. C.; Kanatzidis, M. G., Structural Diversity in White-Light-Emitting Hybrid Lead Bromide Perovskites. *J. Am. Chem. Soc.* **2018,** *140* (40), 13078–13088.
7. Morad, V.; Shynkarenko, Y.; Yakunin, S.; Brumberg, A.; Schaller, R. D.; Kovalenko, M. V., Disphenoidal Zero-Dimensional Lead, Tin, and Germanium Halides: Highly Emissive Singlet and Triplet Self-Trapped Excitons and X-ray Scintillation. *J. Am. Chem. Soc.* **2019,** *141* (25), 9764–9768.
8. Yangui, A.; Roccanova, R.; Wu, Y.; Du, M.-H.; Saparov, B., Highly Efficient Broad-Band Luminescence Involving Organic and Inorganic Molecules in a Zero-Dimensional Hybrid Lead Chloride. *J. Phys. Chem. C* **2019,** *123* (36), 22470–22477.
9. Han, Y.; Li, Y.; Wang, Y.; Cao, G.; Yue, S.; Zhang, L.; Cui, B. B.; Chen, Q., From Distortion to Disconnection: Linear Alkyl Diammonium Cations Tune Structure and Photoluminescence of Lead Bromide Perovskites. *Adv. Opt. Mater.* **2020,** *8*, 1902051.
10. Wu, X.; Trinh, M. T.; Niesner, D.; Zhu, H.; Norman, Z.; Owen, J. S.; Yaffe, O.; Kudisch, B. J.; Zhu, X. Y., Trap states in lead iodide perovskites. *J. Am. Chem. Soc.* **2015,** *137* (5), 2089–2096.
11. Yuan, Z.; Zhou, C.; Tian, Y.; Shu, Y.; Messier, J.; Wang, J. C.; van de Burgt, L. J.; Kountouriotis, K.; Xin, Y.; Holt, E.; Schanze, K.; Clark, R.; Siegrist, T.; Ma, B., One-dimensional organic lead halide perovskites with efficient bluish white-light emission. *Nat. Commun.* **2017,** *8*.
12. Zhou, C.; Worku, M.; Neu, J.; Lin, H.; Tian, Y.; Lee, S.; Zhou, Y.; Han, D.; Chen, S.; Hao, A.; Djurovich, P. I.; Siegrist, T.; Du, M.-H.; Ma, B., Facile Preparation of Light Emitting Organic Metal Halide Crystals with Near-Unity Quantum Efficiency. *Chem. Mater.* **2018,** *30* (7), 2374–2378.
13. Zhou, C.; Tian, Y.; Yuan, Z.; Lin, H.; Chen, B.; Clark, R.; Dilbeck, T.; Zhou, Y.; Hurley, J.; Neu, J.; Besara, T.; Siegrist, T.; Djurovich, P.; Ma, B., Highly Efficient Broadband Yellow Phosphor Based on Zero-Dimensional Tin Mixed-Halide Perovskite. *ACS Appl. Mater. Interfaces* **2017,** *9* (51), 44579–44583.
14. Smith, M. D.; Karunadasa, H. I., White-Light Emission from Layered Halide Perovskites. *Acc. Chem. Res.* **2018,** *51* (3), 619–627.
15. Gautier, R.; Massuyeau, F.; Galnon, G.; Paris, M., Lead Halide Post-Perovskite-Type Chains for High-Efficiency White-Light Emission. *Adv. Mater.* **2019,** *31* (14), e1807383.
16. Cheng, Z.; Lin, J., Layered organic–inorganic hybrid perovskites: structure, optical properties, film preparation, patterning and templating engineering. *CrystEngComm* **2010,** *12* (10).
17. Dohner, E. R.; Hoke, E. T.; Karunadasa, H. I., Self-assembly of broadband white-light emitters. *J. Am. Chem. Soc.* **2014,** *136* (5), 1718–1721.
18. Dohner, E. R.; Jaffe, A.; Bradshaw, L. R.; Karunadasa, H. I., Intrinsic White-Light Emission from Layered Hybrid Perovskites. *J. Am. Chem. Soc.* **2014,** *136* (38), 13154–13157.
19. Neogi, I.; Bruno, A.; Bahulayan, D.; Goh, T. W.; Ghosh, B.; Ganguly, R.; Cortecchia, D.; Sum, T. C.; Soci, C.; Mathews, N.; Mhaisalkar, S. G., Broadband-Emitting 2 D Hybrid Organic-Inorganic Perovskite Based on Cyclohexane-bis(methylamonium) Cation. *ChemSusChem* **2017,** *10* (19), 3765–3772.
20. Hu, H.; Morris, S. A.; Qiao, X.; Zhao, D.; Salim, T.; Chen, B.; Chia, E. E. M.; Lam, Y. M., Molecular engineering of two-dimensional hybrid perovskites with broadband emission for white light-emitting diodes. *J. Mater. Chem. C* **2018,** *6* (38), 10301–10307.
21. Cortecchia, D.; Yin, J.; Petrozza, A.; Soci, C., White light emission in low-dimensional perovskites. *J. Mater. Chem. C* **2019,** *7* (17), 4956–4969.
22. Williams, R. T.; Song, K. S., The Self-Trapped Exciton. *J. Phys. Chem. Solids* **1990**, *51*, 679–716.
23. Cortecchia, D.; Neutzner, S.; Srimath Kandada, A. R.; Mosconi, E.; Meggiolaro, D.; De Angelis, F.; Soci, C.; Petrozza, A., Broadband Emission in Two-Dimensional Hybrid Perovskites: The Role of Structural Deformation. *J. Am. Chem. Soc.* **2016,** *139* (1), 39–42.
24. Cortecchia, D.; Yin, J.; Bruno, A.; Lo, S.-Z. A.; Gurzadyan, G. G.; Mhaisalkar, S.; Brédas, J.-L.; Soci, C., Polaron self-localization in white-light emitting hybrid perovskites. *J. Mater. Chem. C* **2017**, *5* (11), 2771–2780.
25. Booker, E. P.; Thomas, T. H.; Quarti, C.; Stanton, M. R.; Dashwood, C. D.; Gillett, A. J.; Richter, J. M.; Pearson, A. J.; Davis, N.; Sirringhaus, H.; Price, M. B.; Greenham, N. C.; Beljonne, D.; Dutton, S. E.; Deschler, F., Formation of Long-Lived Color Centers for Broadband Visible Light Emission in Low-Dimensional Layered Perovskites. *J. Am. Chem. Soc.* **2017**, *139* (51), 18632–18639.
26. Zhou, C.; Lin, H.; Shi, H.; Tian, Y.; Pak, C.; Shatruk, M.; Zhou, Y.; Djurovich, P.; Du, M.-H.; Ma, B., A Zero-Dimensional Organic Seesaw-Shaped Tin Bromide with Highly Efficient Strongly Stokes-Shifted Deep-Red Emission. *Angew. Chem. Int. Ed.* **2018,** *57* (4), 1021–1024.
27. Zhou, C.; Lin, H.; Tian, Y.; Yuan, Z.; Clark, R.; Chen, B.; van de Burgt, L. J.; Wang, J. C.; Zhou, Y.; Hanson, K.; Meisner, Q. J.; Neu, J.; Besara, T.; Siegrist, T.; Lambers, E.; Djurovich, P.; Ma, B., Luminescent zero-dimensional organic metal halide hybrids with near-unity quantum efficiency. *Chem. Sci.* **2018,** *9* (3), 586–593.
28. Li, M.; Zhou, J.; Zhou, G.; Molokeev, M. S.; Zhao, J.; Morad, V.; Kovalenko, M. V.; Xia, Z., Hybrid Metal Halides with Multiple Photoluminescence Centers. *Angew. Chem. Int. Ed.* **2019,** *58* (51), 18670–18675.
29. Lin, H.; Zhou, C.; Neu, J.; Zhou, Y.; Han, D.; Chen, S.; Worku, M.; Chaaban, M.; Lee, S.; Berkwits, E.; Siegrist, T.; Du, M. H.; Ma, B., Bulk Assembly of Corrugated 1D Metal Halides with Broadband Yellow Emission. *Adv. Opt. Mater.* **2019,** *7* (6), 1801474.
30. Yuan, H.; Massuyeau, F.; Gautier, N.; Kama, A. B.; Faulques, E.; Chen, F.; Shen, Q.; Zhang, L.; Paris, M.; Gautier, R., Doped Lead Halide White Phosphors for Very High Efficiency and Ultra-High Color Rendering. *Angew. Chem. Int. Ed.* **2020,** *59* (7), 2802–2807.
31. Zhang, Y.-L.; Wang, G.-B., Large-Size crystal based on rare earth-free Cu(I) hybrid trigger yellow light with high emissive quantum yields. *J. Mol. Struct.* **2019,** *1183*, 241–245.
32. Yangui, A.; Roccanova, R.; McWhorter, T. M.; Wu, Y.; Du, M.-H.; Saparov, B., Hybrid Organic–Inorganic Halides $(C_5H_7N_2)_2MBr_4$ (M = Hg, Zn) with High Color Rendering Index and High-Efficiency White-Light Emission. *Chem. Mater.* **2019,** *31* (8), 2983–2991.
33. Jiang, C.; Zhong, N.; Luo, C.; Lin, H.; Zhang, Y.; Peng, H.; Duan, C. G., $(Diisopropylammonium)_2MnBr_4$: a multifunctional ferroelectric with efficient green-emission and excellent gas sensing properties. *Chem. Commun.* **2017,** *53* (44), 5954–5957.
34. Dang, Y.; Zhong, C.; Zhang, G.; Ju, D.; Wang, L.; Xia, S.; Xia, H.; Tao, X., Crystallographic Investigations into Properties of Acentric Hybrid Perovskite Single Crystals $NH(CH_3)_3SnX_3$ (X = Cl, Br). *Chem. Mater.* **2016,** *28* (19), 6968–6974.
35. Jalilian, E.; Lidin, S., Size matters—sometimes. The $[Cu_xI_y]_{(y-x)}$-$(NR_4)_{+(y-x)}$ systems. *CrystEngComm* **2011,** *13* (19).
36. You et al., An organic-inorganic perovskite ferroelectric with large piezoelectric response. *Science* **2017**, *357*, 306–309.
37. Hua, X. N.; Liao, W. Q.; Tang, Y. Y.; Li, P. F.; Shi, P. P.; Zhao, D.; Xiong, R. G., A Room-Temperature Hybrid Lead Iodide

Perovskite Ferroelectric. *J. Am. Chem. Soc.* **2018,** *140* (38), 12296–12302.
38. Bakthavatsalam, R.; Haris, M. P. U.; Shaikh, S. R.; Lohar, A.; Mohanty, A.; Moghe, D.; Sharma, S.; Biswas, C.; Raavi, S. S. K.; Gonnade, R. G.; Kundu, J., Ligand Structure Directed Dimensionality Reduction (2D →1D) in Lead Bromide Perovskite. *J. Phys. Chem. C* **2019,** *124* (3), 1888–1897.
39. Mousdis, G. A.; Ganotopoulos, N.-M.; Barkaoui, H.; Abid, Y.; Psycharis, V.; Savvidou, A.; Raptopoulou, C. P., One-Dimensional Organic-Inorganic Hybrid Materials Based on Antimony. *Eur. J. Inorg. Chem.* **2017,** *2017* (28), 3401–3408.
40. Li, S. L.; Zhang, F. Q.; Zhang, X. M., An organic-ligand-free thermochromic luminescent cuprous iodide trinuclear cluster: evidence for cluster centered emission and configuration distortion with temperature. *Chem. Commun.* **2015,** *51* (38), 8062–8065.
41. Goforth, A. M.; Smith, M. D.; Peterson, L.; zur Loye, H-C., Preparation and Characterization of Novel Inorganic–Organic Hybrid Materials Containing Rare, Mixed-Halide Anions of Bismuth(III) *Inorg. Chem.* **2004**, *43* (22), 7042–7049.
42. Bi, W.; Leblanc, N.; Mercier, N.; Auban-Senzier, P.; Pasquier, C., Thermally Induced Bi(III) Lone Pair Stereoactivity: Ferroelectric Phase Transition and Semiconducting Properties of (MV)$BiBr_5$(MV= methylviologen). *Chem. Mater.* **2009,** *21* (18), 4099–4101.
43. Jung, M.-H., Broadband white light emission from one-dimensional zigzag edge-sharing perovskite. *New J. Chem.* **2020,** *44* (1), 171–180.
44. Cui, B. B.; Han, Y.; Huang, B.; Zhao, Y.; Wu, X.; Liu, L.; Cao, G.; Du, Q.; Liu, N.; Zou, W.; Sun, M.; Wang, L.; Liu, X.; Wang, J.; Zhou, H.; Chen, Q., Locally collective hydrogen bonding isolates lead octahedra for white emission improvement. *Nat. Commun.* **2019,** *10* (1), 5190.
45. Febriansyah, B.; Koh, T. M.; John, R. A.; Ganguly, R.; Li, Y.; Bruno, A.; Mhaisalkar, S. G.; England, J., Inducing Panchromatic Absorption and Photoconductivity in Polycrystalline Molecular 1D Lead-Iodide Perovskites through π-Stacked Viologens. *Chem. Mater.* **2018,** *30* (17), 5827–5830.
46. Febriansyah, B.; Lekina, Y.; Ghosh, B.; Harikesh, P. C.; Koh, T. M.; Li, Y.; Shen, Z.; Mathews, N.; England, J., Molecular Engineering of Pure 2D Lead-Iodide Perovskite Solar Absorbers Displaying Reduced Band Gaps and Dielectric Confinement. *ChemSusChem* **2020,** *13*, 1–10.
47. Febriansyah, B.; Giovanni, D.; Ramesh, S.; Koh, T. M.; Li, Y.; Sum, T. C.; Mathews, N.; England, J., Inducing formation of a corrugated, white-light emitting 2D lead-bromide perovskite via subtle changes in templating cation. *J. Mater. Chem. C* **2020,** *8* (3), 889–893.
48. Duan, H. B.; Yu, S. S.; Liu, S. X.; Zhang, H., An inorganic-organic hybrid crystal with a two-step dielectric response and thermochromic luminescence. *Dalton Trans.* **2017,** *46* (7), 2220–2227.
49. Duan, H. B.; Yu, S. S.; Tong, Y. B.; Zhou, H.; Ren, X. M., Two in one: switchable ion conductivity and white light emission integrated in an iodoplumbate-based twin chain hybrid crystal. *Dalton Trans.* **2016,** *45* (11), 4810–4818.
50. Mitzi, D. B., Templating and structural engineering in organic–inorganic perovskites. *J. Chem. Soc., Dalton Trans.* **2001,** *1*, 1–12.
51. SAINT and SADABS; Bruker AXS Inc.: Madison, WI, (2007).
52. Sheldrick, G. M. SHELXL-97, Program for crystal structure refinement; Göttingen, **1997**.
53. Sheldrick, G. M. Acta Crystallogr., *Sect. A: Found. Crystallogr*. **2008**, *64*, 112–122.
54. Momma, K.; Izumi, F., An Integrated Three-Dimensional Visualization System VESTA Using wxWidgets. *Commission on Crystallogr. Comput.* **2006**, *7*, 106–119.
55. Kresse, G.; Furthmuller, J. Efficient Iterative Schemes for Ab initio Total-energy Calculations Using a Plane-wave Basis Set *Phys. Rev. B* **1996**, *54*, 11169–11186.
56. Perdew, J. P.; Burke, K.; Ernzerhof, M. Generalized Gradient Approximation Made Simple. *Phys. Rev. Lett.* **1996**, *77*, 3865–3868.
57. Blochl, P. E., Projector augmented-wave method. *Phys. Rev. B* **1994,** *50* (24), 17953–17979.
58. Kresse, G. and Joubert, D., From ultrasoft pseudopotentials to the projector augmented-wave method. *Phys. Rev. B* **1999,** *59* (3), 1758–1775.
59. Blochl, P. E.; Jepsen, O.; Andersen, O. K., Improved tetrahedron method for Brillouin-zone integrations. *Phys. Rev. B* **1994,** *49* (23), 16223–16233
60. Thirumurugan, A.; Rao, C. N. R., Supramolecular Organization in Lead Bromide Salts of Imidazolium-Based Ionic Liquids. *Cryst. Growth Des.* **2008**, *8*, 1640–1644.
61. Pan, J.; Sun, A.-H.; Han, S.-D.; Wei, L.; Li, J.-H.; Wang, G.-M., Low-Dimensional Lead(II) Halides with In Situ Generated Tripyridine-Derivatives as Countercations: Synthesis, Structures and Properties. *J. Clust. Sci.* **2017,** *28* (5), 2669–2679.
62. Zhou, J.; Li, M.; Ning, L.; Zhang, R.; Molokeev, M. S.; Zhao, J.; Yang, S.; Han, K.; Xia, Z., Broad-Band Emission in a Zero-Dimensional Hybrid Organic [$PbBr_6$] Trimer with Intrinsic Vacancies. *J. Phys. Chem. Lett.* **2019,** *10* (6), 1337–1341.
63. Niemann, R. G.; Kontos, A. G.; Palles, D.; Kamitsos, E. I.; Kaltzoglou, A.; Brivio, F.; Falaras, P.; Cameron, P. J., Halogen Effects on Ordering and Bonding of CH_3NH_{3+} in $CH_3NH_3PbX_3$ (X = Cl, Br, I) Hybrid Perovskites: A Vibrational Spectroscopic Study. *J. Phys. Chem. C* **2016,** *120* (5), 2509–2519.
64. Robinson, K.; Gibbs, G. V.; Ribbe, P. H., Quadratic Elongation: a Quantitative Measure of Distortion in Coordination Polyhedral. *Science* **1971**, *172*, 567–570.
65. Mao, L.; Wu, Y.; Stoumpos, C. C.; Wasielewski, M. R.; Kanatzidis, M. G., White-Light Emission and Structural Distortion in New Corrugated Two-Dimensional Lead Bromide Perovskites. *J. Am. Chem. Soc.* **2017,** *139* (14), 5210–5215.
66. Wang, S.; Yao, Y.; Kong, J.; Zhao, S.; Sun, Z.; Wu, Z.; Li, L.; Luo, J., Highly efficient white-light emission in a polar two-dimensional hybrid perovskite. *Chem. Commun.* **2018,** *54* (32), 4053–4056.
67. Neogi, I.; Bruno, A.; Bahulayan, D.; Goh, T. W.; Ghosh, B.; Ganguly, R.; Cortecchia, D.; Sum, T. C.; Soci, C.; Mathews, N.; Mhaisalkar, S. G., Broadband-Emitting 2 D Hybrid Organic-Inorganic Perovskite Based on Cyclohexane-bis(methylamonium) Cation. *ChemSusChem* **2017,** *10* (19), 3765–3772.
68. Zhou, C.; Lin, H.; Worku, M.; Neu, J.; Zhou, Y.; Tian, Y.; Lee, S.; Djurovich, P.; Siegrist, T.; Ma, B., Blue Emitting Single Crystalline Assembly of Metal Halide Clusters. *J. Am. Chem. Soc.* **2018,** *140* (41), 13181-13184.
69. Baldo, M. A.; O'Brien, D. F.; You, Y.; Shoustikov, A.; Sibley, S.; Thompson, M. E.; Forrest, S. R., *Nature*, **1998,** *395*, 151–154.
70. Lee, S.; Zhou, C.; Neu, J.; Beery, D.; Arcidiacono, A.; Chaaban, M.; Lin, H.; Gaiser, A.; Chen, B.; Albrecht-Schmitt, T. E.; Siegrist, T.; Ma, B., Bulk Assemblies of Lead Bromide Trimer Clusters with Geometry-Dependent Photophysical Properties. *Chem. Mater.* **2019,** *32* (1), 374–380.
71. Chong, W. K.; Giovanni, D.; Sum, T. C., Excitonics in 2D Perovskites. In *Halide Perovskites: Photovoltaics, Light Emitting Devices, and Beyond*; Sum, T. C., Mathews, N.; Wiley-VCH Verlag GmbH & Co. KGaA: Weinheim, **2019**; 55–79.
72. Miller, M. T.; Gantzel, P. K.; Karpishin, T. B., Structures of the Copper(I) and Copper(II) Complexes of 2,9-Diphenyl-1,10-phenanthroline: Implications for Excited-State Structural Distortion. *Inorg. Chem.*, **1998,** *37*, 2285–2290

73. Shaw, G. B.; Grant, C. D.; Shirota, H.; Castner, E. W.; Meyer, G. J.; Chen, L. X., Ultrafast structural rearrangements in the MLCT excited state for copper(I) bis-phenanthrolines in solution. *J. Am. Chem. Soc.*, **2007,** *129*, 2147–2160.
74. Mel'nikov, M. Y.; Weinstein, J. A., Structural reorganization in the excited state of transition metal complexes. *High Energy Chem.* **2008,** *42* (4), 287–289.
75. Zhou, C.; Tian, Y.; Yuan, Z.; Han, M.; Wang, J.; Zhu, L.; Tameh, M. S.; Huang, C.; Ma, B., Precise Design of Phosphorescent Molecular Butterflies with Tunable Photoinduced Structural Change and Dual Emission. *Angew. Chem. Int. Ed.* **2015,** *54* (33), 9591–9595.

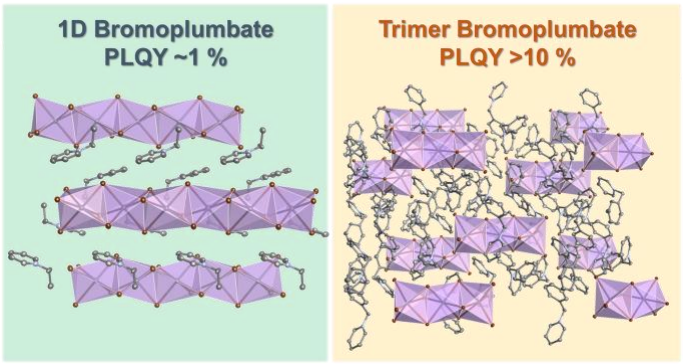
1D Bromoplumbate
PLQY ~1 %
Trimer Bromoplumbate
PLQY >10 %